PHYSICAL REVIEW B **91**, 081101(R) (2015)

Electronic origin of the volume collapse in cerium

N. Devaux,[1] M. Casula,[2,*] F. Decremps,[1] and S. Sorella[3,†]

[1]*Institut de Minéralogie, de Physique des Matériaux et de Cosmochimie, Université Pierre et Marie Curie, case 115, 4 place Jussieu, 75252, Paris cedex 05, France*

[2]*CNRS and Institut de Minéralogie, de Physique des Matériaux et de Cosmochimie, Université Pierre et Marie Curie, case 115, 4 place Jussieu, 75252, Paris cedex 05, France*

[3]*International School for Advanced Studies (SISSA) Via Beirut 2,4 34014 Trieste, Italy and INFM Democritos National Simulation Center, Trieste, Italy*

(Received 4 August 2014; revised manuscript received 14 January 2015; published 2 February 2015)

The cerium α-γ phase transition is characterized by means of a many-body Jastrow-correlated wave function, which minimizes the variational energy of the first-principles scalar-relativistic Hamiltonian, and includes correlation effects in a nonperturbative way. Our variational ansatz accurately reproduces the structural properties of the two phases, and proves that even at temperature $T = 0$ K the system undergoes a first-order transition, with *ab initio* parameters which are seamlessly connected to the ones measured by experiment at finite T. We show that the transition is related to a complex rearrangement of the electronic structure, with a key role played by the p-f hybridization. The underlying mechanism unveiled by this work can hold in many Ce-bearing compounds, and more generally in other f-electron systems.

DOI: 10.1103/PhysRevB.91.081101 PACS number(s): 71.15.−m, 02.70.Ss, 71.20.Eh, 71.27.+a

Understanding the anomalous behavior of cerium, the prototypical f-electron system, is one of the main challenges in condensed-matter physics. The $4f$ electrons are strongly localized and their on-site Coulomb repulsion is large compared to bandwidth. Among all lanthanides, cerium is particularly fascinating, due to the strong hybridization with the $6s6p5d$ bands, all present at the Fermi level. The origin of the cerium volume collapse along the isostructural α-γ transition has been a puzzle since its discovery in 1927 [1]. A microscopic comprehensive description of the transition is still lacking, because a direct comparison with the measured structural properties requires an accuracy below 10 meV. This challenges any *ab initio* method, particularly in a regime of strong correlation. Model calculations have been performed in the Mott [2], Kondo [3,4], and dynamical mean field theory (DMFT) [5–9] frameworks, with input parameters either chosen *ad hoc* or derived from first-principles density functional theory (DFT) and constrained random phase approximation calculations [10]. Fully first-principle electronic structure schemes, such as DFT [11] or GW [12], grasp some features of the α and γ phases, but the quantitative agreement with experiment is generally quite poor.

Experimentally, pure cerium undergoes the α-γ transition always at finite temperature T. Recently, very accurate x-ray-diffraction measurements undoubtedly confirmed the first-order $Fm\bar{3}m$ isostructural character of the transition [13]. The first-order line extrapolates to zero T at negative pressures. Nevertheless, the $T = 0$ K determination of its phase diagram is extremely important as it can shed light on the underlying electronic structure mechanism of the transition, and clarify some critical points still under debate. For instance, some experiments with cerium alloys seem to find a critical low-T end point on the α-γ phase boundary [14], where the effect of alloying is expected to provide a negative chemical pressure on the cerium sites. However, it has also been proven that the end point of the critical line can be tuned down to zero T by changing the bulk modulus through alloying, thus opening the way of new low-T scenarios, like superconducting and non-Fermi-liquid fluctuations [15]. The presence of a low-T end point is obviously material dependent and it is therefore possible that cerium allows instead a genuine f-electron driven 0-K quantum phase transition in the negative pressure side of its phase diagram.

In this Rapid Communication, we present a detailed analysis of the electronic structure modification across the volume collapse, studied from first principles, by means of an explicitly correlated many-body wave function and accurate 0-K quantum Monte Carlo (QMC) techniques. Remarkably, we have been able to stabilize two distinct coexisting solutions, α and γ, with the full set of structural parameters across the transition seamlessly connected to the experimental values at finite T. We prove that the transition results from a subtle competition between local Coulomb repulsion and bandwidth, the latter determined mainly by the a_{1g} and t_{1u} atomic orbitals. The key role is played by the p-f hybridization, set by the octahedral crystal field, which allows the t_{1u} orbital to breathe between the two phases. In the γ phase, the chemical bond has weaker a_{1g} and stronger t_{1u} channels, due to more extended t_{1u} orbitals, if compared to the α phase at the same volume. This weakens the bond strength while it reduces the on-site Coulomb repulsion, resulting in a stabilization of the γ phase at larger volumes.

In our approach, the two phases are described by a paramagnetic Jastrow-correlated Slater determinant (JSD) wave function sampled by QMC techniques:

$$\Psi_{\mathrm{JSD}}(\mathbf{R}_{\mathrm{el}}) = \exp[-J(\mathbf{R}_{\mathrm{el}})]\,\det[\phi_i(\mathbf{r}_j)], \tag{1}$$

where $1 \leqslant i,j \leqslant N$, $\mathbf{R}_{\mathrm{el}} = \{\mathbf{r}_1 \ldots,\mathbf{r}_N\}$ is the many-body N-electron configuration, and the determinant is factorized in two spin components $\uparrow$ and $\downarrow$, since the molecular orbitals ϕ_i have a definite spin projection along z. Both J and ϕ are

*michele.casula@impmc.upmc.fr
†sorella@sissa.it

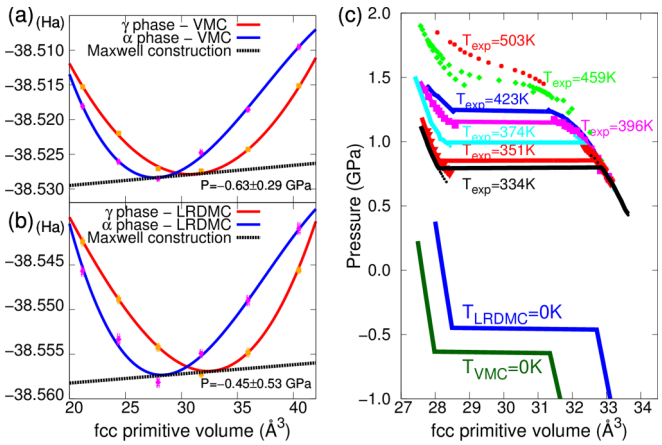

FIG. 1. (Color online) Panels (a) and (b): Equation of states of the α and γ phases obtained by VMC and LRDMC calculations, respectively. The black dashed straight line is the Maxwell construction with the corresponding calculated α-γ transition pressure. (c) Clapeyron diagram obtained at 0 K in quantum Monte Carlo, compared to the experimental phase diagram by Decremps *et al.* [13] at finite T. Remarkably, the upper and lower critical volumes are within the experimental range of the coexistence region.

analytic functions with parameters that minimize the energy of the scalar-relativistic first-principles Hamiltonian (see [16] for details). The full Coulomb electron-ion interaction is replaced by a scalar-relativistic Hartree-Fock energy consistent pseudopotential [17] with $5s^2 5p^6 6s^2 5d^1 4f^1$ atomic reference configuration, which includes semicore states.

The Jastrow factor takes into account strong local correlations as well as intersite correlations, and thoroughly modifies the DFT generated Slater determinant. We fully optimized the JSD wave function in a 32-atom cubic supercell with periodic boundary conditions, which yields structural parameters close to the thermodynamic limit (see the Supplemental Material in [16]). By determining the variational energy as a function of the unit-cell volume, we evaluated the equation of states at the variational Monte Carlo level (VMC), as reported in Fig. 1(a). The *fcc* equilibrium volume per atom $V_{\rm eq}$ of the α phase turns out to be 27.4 Å^3, in an agreement with the experimental value (28.82 Å^3) [18] greatly better than local-density approximation (LDA) or generalized gradient approximation (GGA) DFT calculations. To further improve the electronic structure, we used the lattice regularized diffusion Monte Carlo (LRDMC) method [19,20]. In the LRDMC, the starting point is our best VMC wave function given by (1), that is projected to the ground state with the approximation of the fixed nodes, pinned to the ones of the VMC wave function to cope with the sign problem arising in the imaginary time projection. The LRDMC equation of states plotted in Fig. 1(b) yields an equilibrium volume of 28.4 Å^3, in very good agreement with experiment, while the bulk modulus B is overestimated (see Table I).

By starting from the optimal JSD wave function for the α phase, we performed VMC energy minimizations at much larger volumes (>40 Å), where we stabilized a second paramagnetic solution, lower in energy than the α phase. This second solution holds out even at smaller volumes, although at higher energies. Our computer simulations then reproduced what is

TABLE I. Structural and phase-transition parameters for α and γ phases obtained by VMC and LRDMC, compared with the experiment. The α-γ phase transition parameters are taken from Ref. [13] at $T = 334$ K. A further detailed comparison with alternative *ab initio* methods is reported in the Supplemental Material [16].

	VMC ($T = 0$ K)	LRDMC ($T = 0$ K)	Expt.
$V_{\rm eq}^{\alpha}$ (Å^3)	27.4 ± 0.1	28.4 ± 0.2	28.52 [18]
$V_{\rm eq}^{\gamma}$ (Å^3)	30.8 ± 0.2	32.3 ± 0.3	34.35 [21]
B^{α} (GPa)	48 ± 1	50 ± 3	35 [22]
B^{γ} (GPa)	38 ± 1	45 ± 3	21–24 [23,24]
$V_{\rm min}$ (Å^3)	28.0 ± 0.2	28.5 ± 0.3	28.2 [13]
$V_{\rm max}$ (Å^3)	31.3 ± 0.3	32.7 ± 0.4	32.8 [13]
δV (%)	11.7 ± 0.6	13.8 ± 1.1	15.1 [13]
p_t (GPa)	−0.63 ± 0.29	−0.45 ± 0.53	0.7 [13]
ΔU (meV)	13 ± 1	12 ± 3	25 [13]

seen in experiment, with a clear hysteresis between the two states as a function of volume [see Fig. 1(c)]. Further analysis, based on the Maxwell common tangent construction and on the geometry parameters, confirmed that this solution is fully compatible with the sought γ phase. Its LRDMC equilibrium volume is 32.3 Å^3 (Table I), representing a volume collapse of about 13%; its bulk modulus is softened with respect to the α phase (as seen in experiments); the (negative) transition pressure p_t is compatible with the extrapolated transition line to the negative side of the experimental p-T diagram; and the lower $V_{\rm min}$ and upper $V_{\rm max}$ critical volumes are within the experimental range of phase coexistence [Fig. 1(c) and Table I].

Once the macroscopic parameters are determined, our theoretical approach is qualified to provide the microscopic physical origin of the volume collapse transition. By QMC methods it is actually possible to directly access spin and charge fluctuations, through the measure of the spin-spin and charge-charge correlation functions. Here, we define the charge and spin operators on a cerium site as $\hat{n}_i = \int_{V(\mathbf{R}_i)} d\mathbf{r}[\psi_\uparrow^\dagger(\mathbf{r})\psi_\uparrow(\mathbf{r}) + \psi_\downarrow^\dagger(\mathbf{r})\psi_\downarrow(\mathbf{r})]$ and $\hat{\sigma}_i = 1/2 \int_{V(\mathbf{R}_i)} d\mathbf{r}[\psi_\uparrow^\dagger(\mathbf{r})\psi_\uparrow(\mathbf{r}) - \psi_\downarrow^\dagger(\mathbf{r})\psi_\downarrow(\mathbf{r})]$, where the fermionic field $\psi_\sigma^\dagger(\mathbf{r})$ [$\psi_\sigma(\mathbf{r})$] creates (annihilates) an electron of spin σ at the position $\mathbf{r}$, and the integral is done over a sphere of radius $R = 2.5$ a.u. around the nucleus $\mathbf{R}_i$. At the volume $V = 31.73$ Å^3, which falls into the experimental coexistence region, this integration radius gives $\langle \hat{n}_i \rangle \approx 9$ electrons per site in both phases, mainly coming from the $5s^2 5p^6$ semicore and the $4f$ states, which are the most localized among the valence electrons described by our pseudopotential. The on-site charge fluctuations $\langle \hat{n}_i \hat{n}_i \rangle - \langle \hat{n}_i \rangle \langle \hat{n}_i \rangle$ computed by VMC are 1.32(2) and 1.35(1) for the γ and α phase, respectively. Thus, there is no sizable difference between the two phases. LRDMC does not change this picture. Moreover, the Jastrow parameters which control the charge-charge correlations do not change significantly between the two phases, in accordance with the charge-charge correlation function results. Therefore, no suppression of double occupancies occurs in the γ phase, signaling that the Mott scenario of the α-γ transition should be definitely discarded. This is an important conclusion, considering that the Mott transition has been proposed as

a valid interpretation of the volume collapse until very recently [2,11,25].

In the spin sector $\langle\hat{\sigma}_i\rangle = 0$, because the α and γ wave functions do not break the spin symmetry, as both states are paramagnetic by construction. From the experimental point of view, the cerium *fcc* lattice undergoes the volume collapse between two paramagnetic states at finite temperature. However, the α and γ phases feature a very different magnetic susceptibility, the former being Pauli like, the latter of Curie-Weiss type. Early calculations based on the Kondo model [3] and later LDA + DMFT studies [5–8] explained this difference in terms of Kondo local moment formations in the γ phase, while the effective Kondo temperature of the DMFT impurity problem is much larger in the α phase, leaving it in the fully screened singlet state. Thus, the spin response characterizes the two paramagnetic phases at finite temperature. At 0 K the on-site spin-spin correlation functions $\langle\hat{\sigma}_i\hat{\sigma}_i\rangle - \langle\hat{\sigma}_i\rangle\langle\hat{\sigma}_i\rangle$ computed by VMC yield 0.5614(3) and 0.5861(4) for the γ and α phase, respectively. Moreover, the spin-spin correlations have a very short range. As in the charge sector, there is no significant difference between the two phases. This result can be understood in terms of Kondo physics. $T = 0$ K is lower than any finite Kondo temperature, so that both phases are in the fully screened regime [26].

The most striking difference between the α and γ solutions is in the electron density $\langle\hat{\rho}(x,y,z)\rangle$, computed always at the same volume $V = 31.73$ Å^3. The xy contour plot of $\rho_\alpha - \rho_\gamma$ is presented in Fig. 2(a) for $z = 0$, i.e., at the plane containing the central atom and four nearest neighbors. This shows positive (red) and negative (blue) lobes of atomic character. The Jastrow factor cannot explain this difference on its own, as we have seen that its variation between the two phases is weak. Instead, the difference should come from the Slater determinant $|\Psi^{\rm SD}\rangle = \det[\phi]$, once it is combined and optimized together with the Jastrow factor in (1). This is indeed confirmed by $\rho_\alpha^{\rm SD} - \rho_\gamma^{\rm SD}$, where $\rho^{\rm SD} = \langle\Psi^{\rm SD}|\hat{\rho}|\Psi^{\rm SD}\rangle$ with J dropped (set to 0) and $\Psi^{\rm SD}$ frozen, plotted in Fig. 2(b). The charge density difference carried by the Slater determinant shows a similar pattern than the full many-body JSD density. This is a strong signature that the main difference between the α and γ phases at 0 K comes from a *static* rearrangement of the electronic structure, driven by the *dynamic* electron correlation, which—in our approach—is coded in the Jastrow factor. It is worth pointing out here that both phases share almost the same radial charge density (up to a 0.5% difference) around the nuclei. The main variation is in its angular distribution, suggesting that the transition must be understood in terms of an electron rearrangement at the atomic level, which will consequently affect the chemical bond in the solid.

In order to analyze this hypothesis, we consider the density matrix $D^{\rm proj}(\mathbf{r},\mathbf{r}') = \sum_i \psi_i^{\rm proj}(\mathbf{r})\psi_i(\mathbf{r}')$ left projected over a single cerium atom. This is obtained by expanding the molecular orbitals $\psi_i(\mathbf{r})$ on an atomic basis set and considering in $\psi_i^{\rm proj}(\mathbf{r})$ only the components referring to the chosen atom. We then determine the "best" atomic orbitals $\phi_i^{\rm ANO}(\mathbf{r})$ representing the projected density matrix by $\sum_{i=1}^k \phi_i^{\rm ANO}(\mathbf{r})\psi_i^R(\mathbf{r}')$ in an optimally reduced space, namely in terms of only $k \ll N$ atomic natural orbitals (ANOs) centered on the reference atom and corresponding auxiliary molecular orbitals $\psi_i^R(\mathbf{r}')$ spanning all the cell. This can be achieved by a standard Schmidt decomposition, through a minimization of the Euclidean distance between the truncated and the projected density matrix. The resulting eigenvalues λ_i^2 are such that $|D^{\rm proj}|^2 \approx \sum_{i=1}^k \lambda_i^2$, and they are related to the ANOs occupation and their chemical reactivity (see Supplemental Material in [16]).

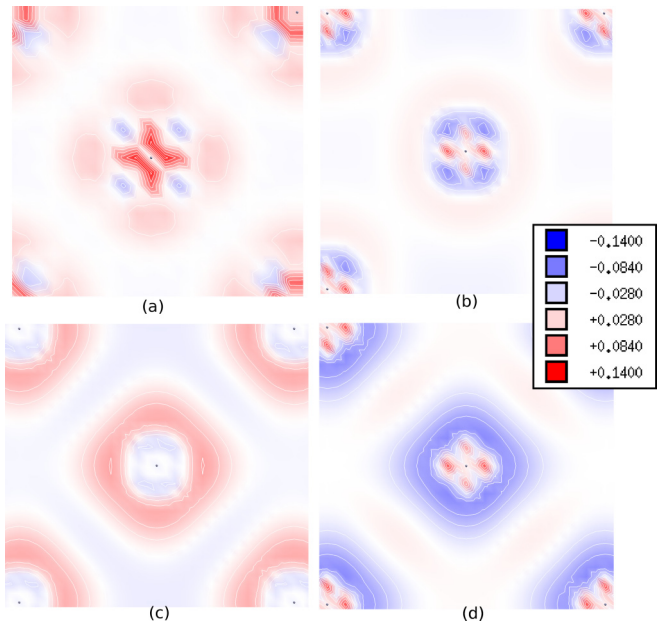

FIG. 2. (Color online) xy contour plot at $z = 0$ (plane containing the central atom). (a) JSD-VMC density difference $\rho_\alpha - \rho_\gamma$; (b) $\rho_\alpha^{\rm SD} - \rho_\gamma^{\rm SD}$ density difference coming from the determinantal part only of the JSD-VMC wave function. Panels (c) and (d) $\delta\rho_i^{\rm SD} = \sum_j\{\rho_\alpha^{\rm SD} - \rho_\gamma^{\rm SD}\}_{ij}$, with $\{\rho^{\rm SD}\}_{ij} = \langle P_i\Psi^{\rm SD}|\hat{\rho}|P_j\Psi^{\rm SD}\rangle$ the projected electron density, where $i = \{s+d, p+f(t_{1u})+f(t_{2u})\}$ are the atomic orbital symmetries for the (c) and (d) panels, respectively. The density values are expressed in Å^{-3}. The JSD-VMC density values are twice smaller than the color-coded scale printed in the key. The unit-cell volume is 31.73 Å^3. The locations of Ce atoms are indicated by gray dots. The nearest neighbors on the plane of the central atom are at the square corners.

Any local atomic variation due to a change in the chemical bond or crystal field is detected by this approach, as it takes into account the embedding of the atom in its environment. In Fig. 3 we plot the ANOs λ_i^2 eigenvalues and their spread, for the same volume as in Fig. 2. The first six ANOs would be perfectly occupied in the case of noninteracting closed-shell pseudoatoms. In particular, the first four are the semicore states.

Two striking features are apparent. First, between the α and γ ANOs, there is the variation of the seventh atomic orbital weight. In the α phase the seventh ANO, of a_{1g} symmetry, has almost the same weight as the fifth and sixth ANOs, of e_g symmetry arising from $5d_{3z^2-r^2}$ and $5d_{x^2-y^2}$ orbitals, degenerate in the octahedral crystal field. As the isolated atomic ground state is in the ^1G singlet $6s^2 5d^1 4f^1$ configuration (with the s shell full and inert), it is clear that the s-to-d atomic promotion is crucial to explain the chemical bond in the α phase, with the two e_g ($5d$) and the a_{1g} ($6s$) orbitals cooperating to set its strength. The cooperative action

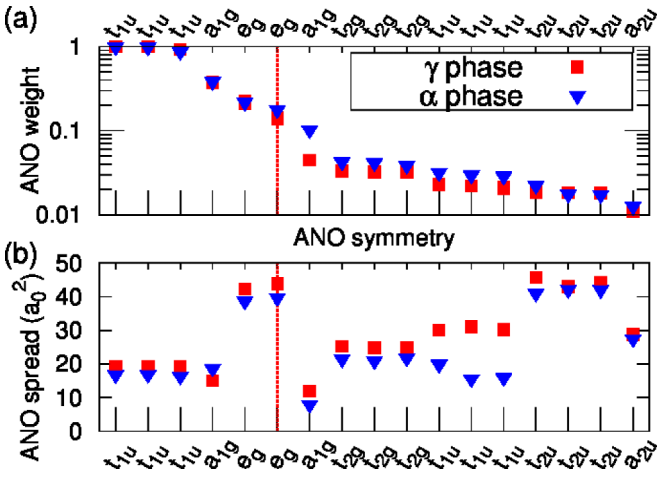

FIG. 3. (Color online) Left panel: First 17 ANO eigenvalues of the density matrix Schmidt decomposition for the α and γ phases at $V = 31.73$ Å^3. Their symmetry is reported in the x axis. The vertical red line represents the filling (6) of a noninteracting closed-shell pseudoatom in the octahedral field. The variation between the two phases is remarkable for the a_{1g} (atomic $6s$) seventh eigenvalue, which is more resonating with the ones below in the α phase. Right panel: natural orbital localization measured by the spread $\Omega = \langle\Psi|r^2|\Psi\rangle - |\langle\Psi|\mathbf{r}|\Psi\rangle|^2$. Note that the largest difference comes from the t_{1u} orbitals.

of s and d orbitals has been highlighted also in the formation of the Ce dimer [27,28].

On the other hand, in the γ phase, the a_{1g} ($6s$) ANO weight is almost an order of magnitude smaller. It means that the s character of the outer-shell region is weaker in γ than in α, as shown also by the density variation $\rho_\alpha^{\mathrm{SD}} - \rho_\gamma^{\mathrm{SD}}$ projected onto the s-atomic orbitals, plotted in Fig. 2(c).

In both α and γ phases, above the seventh a_{1g} ANO, there is a series of orbitals with small eigenvalues but competing each other in magnitude. The remaining atomic f electron shares a mixed character, with non-negligible a_{2u}, t_{2u}, and t_{1u} occupations.

The second important difference between α and γ is the localization of the three degenerate t_{1u} orbitals. The octahedral crystal field makes the t_{1u} orbitals strongly hybridized between the p and f atomic symmetries. It turns out that the spread of the t_{1u} is twice larger in the γ phase, as reported in Fig. 3(b). This is consistent with Fig. 2(d), where the $p + f(t_{1u})$ projected density is spread over a wider range in the γ phase. The larger t_{1u} extension reduces the strong local Coulomb repulsion and increases the overlap with its neighbors and thus its bonding character.

To summarize, the sizable difference between the α and γ chemical bond character results from a reduction of the a_{1g} weight together with an increase of the t_{1u} overlap. The breathing of the t_{1u} orbitals takes place through the hybridization between the p and f states, coupled by the octahedral crystal field. The chemical bond in the γ phase is weaker (and so the equilibrium volume is larger) as the t_{1u}-based bond is less strong than the s-a_{1g} one. On the other hand, the system gains energy by reducing the on-site Coulomb repulsion through more extended t_{1u} orbitals.

In conclusion, the volume collapse transition can be understood at 0 K as a conventional first-order transition of electronic origin. The two phases are well described by the zero-T equation of state, while their relative stability is provided by tiny entropic effects [13]. The underlying mechanism of the volume collapse should survive by the addition of the spin-orbit coupling [29], not present in our calculations, as in cerium it is much weaker than the local Coulomb repulsion, although competing with the crystal-field splitting [30]. Our picture disproves the validity of the Mott model, and puts cerium in a quantum phase transition regime. Our detailed predictions on the interplay between valence and localized orbitals can be experimentally tested by x-ray electron spectroscopy at L edges, to probe the s and p states. The electronic phase transition mechanism detailed in this work can be applied to cerium alloys, and more generally to a wider class of f-electron systems.

We acknowledge useful discussions with S. Biermann, M. Fabrizio, and Ph. Sainctavit. We are indebted to M. Dolg for providing us with his scalar relativistic energy consistent tetravalent cerium pseudopotential. We thank L. Paulatto for helping us with the generation of cerium PAW pseudopotentials by using the quantum-espresso atomic ld1 code. The computational resources used for this work have been provided by PRACE Grant No. 2012061116, and IDRIS/GENCI Grant No. 2014096493.

[1] P. W. Bridgman, Proc. Am. Acad. Arts Sci. **62**, 207 (1927).
[2] B. Johansson, I. A. Abrikosov, M. Aldén, A. V. Ruban, and H. L. Skriver, Phys. Rev. Lett. **74**, 2335 (1995).
[3] J. W. Allen and R. M. Martin, Phys. Rev. Lett. **49**, 1106 (1982).
[4] J. W. Allen and L. Z. Liu, Phys. Rev. B **46**, 5047 (1992).
[5] M. B. Zölfl, I. A. Nekrasov, T. Pruschke, V. I. Anisimov, and J. Keller, Phys. Rev. Lett. **87**, 276403 (2001).
[6] K. Held, A. K. McMahan, and R. T. Scalettar, Phys. Rev. Lett. **87**, 276404 (2001).
[7] K. Haule, V. Oudovenko, S. Y. Savrasov, and G. Kotliar, Phys. Rev. Lett. **94**, 036401 (2005).
[8] B. Amadon, S. Biermann, A. Georges, and F. Aryasetiawan, Phys. Rev. Lett. **96**, 066402 (2006).
[9] J. Bieder and B. Amadon, Phys. Rev. B **89**, 195132 (2014).
[10] F. Nilsson, R. Sakuma, and F. Aryasetiawan, Phys. Rev. B **88**, 125123 (2013).
[11] M. Casadei, X. Ren, P. Rinke, A. Rubio, and M. Scheffler, Phys. Rev. Lett. **109**, 146402 (2012).
[12] R. Sakuma, T. Miyake, and F. Aryasetiawan, Phys. Rev. B **86**, 245126 (2012).
[13] F. Decremps, L. Belhadi, D. L. Farber, K. T. Moore, F. Occelli, M. Gauthier, A. Polian, D. Antonangeli, C. M. Aracne-Ruddle, and B. Amadon, Phys. Rev. Lett. **106**, 065701 (2011).

[14] J. D. Thompson, Z. Fisk, J. M. Lawrence, J. L. Smith, and R. M. Martin, Phys. Rev. Lett. **50**, 1081 (1983).
[15] M. Dzero, M. R. Norman, I. Paul, C. Pepin, and J. Schmalian, Phys. Rev. Lett. **97**, 185701 (2006).
[16] See Supplemental Material at http://link.aps.org/supplemental/10.1103/PhysRevB.91.081101 for correlated wave function and QMC methods, comparison with other computational schemes, finite-size scaling analysis, and calculation of optimal atomic natural orbitals, which includes Refs. [9, 11, 29, 31–44]. (Reference [31] is the first reference in the Supplemental Material not already in this Rapid Communication]. Reference [44] is the last reference in the Supplemental Material not already in this Rapid Communication.)
[17] M. Dolg (private communication).
[18] D. C. Koskenmaki and K. Gschneidner, *Handbook on the Physics and Chemistry of Rare Earths* (North-Holland, Amsterdam, 1978).
[19] M. Casula, C. Filippi, and S. Sorella, Phys. Rev. Lett. **95**, 100201 (2005).
[20] M. Casula, S. Moroni, S. Sorella, and C. Filippi, J. Chem. Phys. **132**, 154113 (2010).
[21] B. J. Beaudry and P. E. Palmer, J. Less-Common Met. **34**, 225 (1974).
[22] J. S. Olsen, L. Gerward, J. P. Dancausse, and E. Gering, Physica B **190**, 92 (1993).
[23] K. A. J. Gschneidner, *Solid State Physics* (Academic Press, New York and London, 1964), Vol. 16, pp. 275–426.
[24] J. Olsen, L. Gerward, U. Benedict, and J.-P. Itié, Physica B+C **133**, 129 (1985).
[25] B. Johansson, A. V. Ruban, and I. A. Abrikosov, Phys. Rev. Lett. **102**, 189601 (2009).
[26] L. dé Medici, A. Georges, G. Kotliar, and S. Biermann, Phys. Rev. Lett. **95**, 066402 (2005).
[27] X. Cao and M. Dolg, Mol. Phys. **101**, 1967 (2003).
[28] B. O. Roos, R. Lindh, P.-A. Malmqvist, V. Veryazov, and P.-O. Widmark, J. Phys. Chem. A **112**, 11431 (2008).
[29] N. Lanatà, Y.-X. Yao, C.-Z. Wang, K.-M. Ho, J. Schmalian, K. Haule, and G. Kotliar, Phys. Rev. Lett. **111**, 196801 (2013).
[30] M. E. Manley, R. J. McQueeney, B. Fultz, T. Swan-Wood, O. Delaire, E. A. Goremychkin, J. C. Cooley, W. L. Hults, J. C. Lashley, R. Osborn *et al.*, Phys. Rev. B **67**, 014103 (2003).
[31] M. Casula, C. Attaccalite, and S. Sorella, J. Chem. Phys. **121**, 7110 (2004).
[32] S. Sorella, M. Casula, and D. Rocca, J. Chem. Phys. **127**, 014105 (2007).
[33] F. Sterpone, L. Spanu, L. Ferraro, S. Sorella, and L. Guidoni, J. Chem. Theory Comput. **4**, 1428 (2008).
[34] S. Sorella, M. Casula, L. Spanu, and A. Dal Corso, Phys. Rev. B **83**, 075119 (2011).
[35] M. Marchi, S. Azadi, and S. Sorella, Phys. Rev. Lett. **107**, 086807 (2011).
[36] M. Casula and S. Sorella, Phys. Rev. B **88**, 155125 (2013).
[37] A. Svane, Phys. Rev. Lett. **72**, 1248 (1994).
[38] Z. Szotek, W. M. Temmerman, and H. Winter, Phys. Rev. Lett. **72**, 1244 (1994).
[39] B. Amadon, J. Phys.: Condens. Matter **24**, 075604 (2012).
[40] C. J. Umrigar, J. Toulouse, C. Filippi, S. Sorella, and R. G. Hennig, Phys. Rev. Lett. **98**, 110201 (2007).
[41] S. Sorella, TurboRVB, Quantum Monte Carlo software for electronic structure calculations, http://people.sissa.it/sorella/web/index.html.
[42] S. Chiesa, D. M. Ceperley, R. M. Martin, and M. Holzmann, Phys. Rev. Lett. **97**, 076404 (2006).
[43] H. Kwee, S. Zhang, and H. Krakauer, Phys. Rev. Lett. **100**, 126404 (2008).
[44] M. Marchi, S. Azadi, M. Casula, and S. Sorella, J. Chem. Phys. **131**, 154116 (2009).